Oceanologia, 67 (4)/2025, 67402
Polish Academy of Sciences
Institute of Oceanology

https://doi.org/10.5697/SUEC1393

Mutual influence of wind-driven flow and the wave bed boundary layer in the remote foreshore of a non-tidal sea

Magdalena Stella-Bogusz[1,*], Rafał Ostrowski[1], Grzegorz R. Cerkowniak[1,2]

Abstract
A new model of the wind-driven current is presented. The solution comprises the stationary flow and wave-driven nearbed oscillatory velocities. The wave-related bed boundary layer causes additional shear stresses that affect the wind-driven current. Both the wave boundary layer (WBL) and the wave–current boundary layer (WCBL) are considered. The bed boundary layer produces a modified logarithmic velocity distribution in the wind-driven current model. The results of modelled profiles are verified by measurement data of wind, wave and current characteristics. All measurements are conducted in the vicinity of the Coastal Research Station (CRS) in Lubiatowo, where wave and current data were collected approximately 2.8 km (1.5 NM) from the coastline, at depth ca. 17 m, whereas the wind parameters were measured on land near the Station. The investigation area hydrodynamics is typical of the south Baltic Sea coast. Reduction of flow velocities near the seabed, particularly distinct under the wave-dominated regime, is the main feature of the new model. The new modified logarithmic profile defining velocity vertical distributions shows good agreement with the measurements. Furthermore, it is confirmed that the wave-induced nearbed turbulence strongly affects the wind-driven current, while the wind-driven current has an insignificant influence on the bed boundary layer.

Keywords
Modified logarithmic velocity distribution; Bed shear stresses; Wave and wave-current bed boundary layers; Wind-driven current

[1] *Institute of Hydro-Engineering, Polish Academy of Sciences, ul. Kościerska 7, 80–328 Gdańsk, Poland*
[2] *University of Gdańsk, Marszałka Piłsudskiego 46, 81–378 Gdynia, Poland*
***Correspondence**: m.stella@ibwpan.gda.pl (M. Stella-Bogusz)

Received: 15 July 2024; **revised:** 8 September 2025; **accepted**: 15 September 2025

1. Introduction

Water motion in the form of waves and sea currents is a driver of sediment transport. Hydrodynamic and lithodynamic processes occurring in various depth zones are interesting not only in the scientific context. The knowledge of the parameters of such processes is useful in the optimization of ventures planned in marine areas, such as the construction of engineering structures and dredging works. The characteristics of water and sediment motion in offshore regions and in the shoreline vicinity are completely different.

Within the nearshore area where tidal impacts are negligible (e.g. the Baltic Sea) and the wave energy is dissipated (mostly by waves breaking in the surf zone), wave-driven currents predominate (longshore and cross-shore currents, including rip currents). In regions located further off the shoreline, water motion is related mainly to flows typically occurring in deep water, such as drift currents or gradient currents.

The remote foreshore zone stretches seawards from the so-called depth of closure, delineating the outer coastal boundary beyond which even extreme storm waves generate neither any intensive motion of seabed sediments nor distinct changes in the sea bottom resulting from this motion (see e.g. Dean, 2002). For the south Baltic coastal zone, the depth of closure, estimated on the basis of long-term bathymetric changes, amounts to 6.0–7.7 m (Cerkowniak et al., 2015a). However, theoretical modelling shows that extremely high storm waves (higher than 3.5 m) can generate sediment movement with a high regime even at depths of 13–15 m (Cerkowniak et al., 2015b).

The south Baltic remote foreshore zone is located at depths of 16–20 m (Stella, 2021). As presented by Stella

(2021), results of measurements of sea bottom level changes over a few months in the area of 2.6 km × 0.53 km show seabed evolution from a few centimetres to tens of centimetres. In addition, bathymetric surveys revealed moveable bed forms 5–20 cm high and 100–200 cm long (the form length is defined as the distance between neighbouring crests or troughs). Such significant symptoms of seabed dynamics beyond the nearshore zone (the surf zone), that is, beyond the depth of closure, can appear only due to the joint impact of high storm waves and strong currents (see e.g. Ostrowski and Stella, 2020). On the basis of a thorough analysis of the long-term wave-current climate and theoretical modelling of the nearbed shear stresses, Ostrowski and Stella (2020) determined conditions sufficient to cause intensive transport of sandy sediments at depths of 16–20 m. It was found that sediment motion of this kind can occur during severe storms due to a nonlinear interaction between nearbed wave-induced oscillatory flows and the current generated by wind. Further, Ostrowski and Stella (2020) discovered that the key role in a theoretical description of this phenomenon is played by the accurate determination of the vertical distribution of the wind-driven current velocity, which is significantly affected by the wave bed boundary layer (WBL).

It is worthwhile mentioning that non-tidal currents (including wind-driven currents) have recently drawn the attention of researchers dealing with seabed dynamics in tidal regions. These currents have been found to significantly influence the appearance and movement of sand waves (Overes et al., 2024).

Beyond specific deep regions, the Coriolis force very weakly affects water flow in the Baltic Sea. In such conditions, the Ekman spiral does not occur, and the wind-driven flow is collinear with the direction of wind, as well as unidirectional with depth (Krauss, 2001; Trzeciak, 2000; Reyes-Hernández and Valle-Levinson, 2010). On the basis of velocity profile measurements within the intermediate depths (about 17 m) of the Baltic Sea, Ostrowski et al. (2018) found that the direction of flow velocities is actually the same in the entire water column, almost identical to the wind direction. Hence, the vertical profile of the wind-driven current can be modelled using a directionally invariable velocity distribution.

The wave-current interaction is a complex phenomenon. Each parameter of the coupled wave–current flow can affect lithodynamic and morphodynamic processes. The angle between the wave propagation direction and the stationary flow influences the shape of seabed forms (Baas et al., 2021), the flow velocity and the impact of the flow itself on the sea bottom (Lacy et al., 2007; Lim and Madsen, 2016), as well as the shear stress and seabed roughness (Malarkey and Davies, 1998; Wiberg, 2005). Investigations of the wave-current motion of water over a rough bed have revealed that the bed boundary layer causes a nonlinear interaction between waves and the steady current; therefore, the resultant shear stresses cannot be determined by superposing wave and current components (Grant and Madsen, 1979; Kemp and Simons, 1982). In the remote foreshore, storm waves can pick up single sand grains from the seabed, but are incapable of inducing intensive sediment transport. A simultaneous occurrence of a current, however, can lead to sediment motion (Grant and Madsen, 1979; Wiberg, 2005). It has also been found that the presence of the WBL increases bottom roughness for currents, and friction coefficients for nearbed currents can grow by as much as an order of magnitude (Wiberg, 2005; Egan et al., 2019).

Chen and Hu (2020) proposed a model predicting the velocity distribution and sediment flux under a steady current interacting with asymmetric waves. Within that approach, the wave-induced and current-related components of the flow were "separated to isolate the wave-current interaction". According to the findings of Chen and Hu (2020), the WBL thickness was distinctly affected by the current and, simultaneously, the wave-related nearbed turbulent viscosity gave rise to a reduction of the flow velocity beyond the WBL.

The logarithmic distribution is a simple theoretical model accurately describing the vertical velocity profile in stationary flows. The logarithmic velocity profile, resulting from the assumption of the linear distribution of the turbulent kinematic viscosity, is commonly applied to rivers (see e.g. Meyer, 2009) and sea currents (Nielsen, 1992, 2009).

1.1 Objectives of the study

To improve this model and achieve better agreement with theoretical and measured velocity profiles, modifications of the logarithmic distribution have been proposed (Nielsen, 1992; Meyer, 2009; Stella et al., 2019). The present study is an attempt at another modification of this kind.

The velocity profile depends on the vertical distribution of the turbulent kinematic viscosity. This distribution can have various shapes (van Rijn, 1993; Zuo et al., 2019). In the proposed approach, the vertical linear distribution of the turbulent kinematic viscosity, which determines the wind-driven velocity profile, is corrected by the inclusion of the WBL. Unlike in the previous modifications (based e.g. on additional apparent bottom roughness), this aim is achieved by assuming that the turbulent kinematic viscosity value at the bottom is other than zero. This quantity is obtained by solving the momentum equation in the WBL or the WCBL. It is believed that the steady current weakly affects the wave boundary layer, while the steady flow is traditionally assumed to remain under the strong influence of the WBL (Nielsen, 1992, 2009). To investigate this problem, both the wave and the wave-current boundary layer are considered.

2. Material and methods

2.1 Site and data

Parameters of wind, waves and currents were measured at the Coastal Research Station (CRS) in Lubiatowo from April 26 to June 30, 2014. CRS Lubiatowo is a field laboratory operated by the Institute of Hydro-Engineering of the Polish Academy of Sciences (IBW PAN), situated on the open seaside, in northern Poland (see Figure 1). The hydrodynamic and lithodynamic parameters in the vicinity of CRS Lubiatowo can be assumed to be representative of the south Baltic coastal zone (Cerkowniak et al., 2017; Ostrowski et al., 2016).

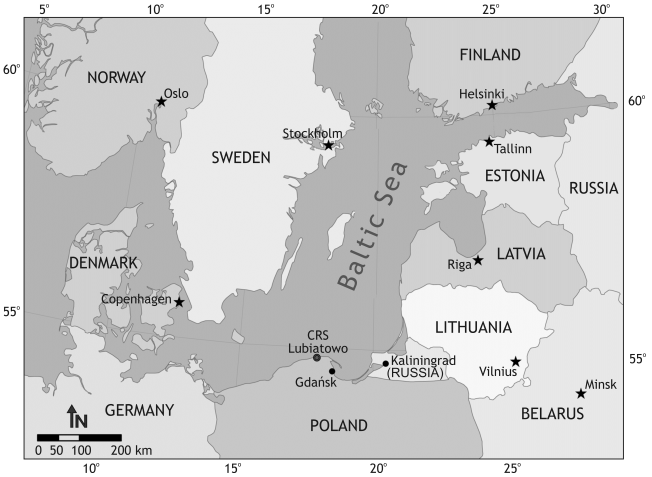

Figure 1. Location of the study site, map generated using CorelDRAW Standard 2021, version 23.0.0.363, https://www.coreldraw.com/pl/product/coreldraw/standard/.

The seabed at the study site is built of fine quartz sand, with a density ρ_s of 2650 kg m^{-3} and a representative grain diameter d_{50} of 0.13 mm. In this region, divers have spotted bedforms with a height of 5–15 cm at intervals of 1–2 m from crest to crest. The cross-shore profile shows a mild slope, with an inclination between 1 and 2%, and 3–4 bars. This morphological situation is favourable for multiple wave breaking, which causes significant wave energy dissipation in the nearshore zone (Pruszak et al., 2008). Figure 2 shows an exemplary cross-section of the shore at CRS Lubiatowo, the depth of closure determined by Cerkowniak et al. (2015a), and the theoretical range of bottom level changes due to wave impact according to Cerkowniak et al. (2015b), as well as an approximate location of the measuring equipment.

Flow velocities and directions, as well as surface wave parameters, were measured by an acoustic current profiler (AWAC). The device, operating at 1000 kHz frequency, was mounted on a frame lying on the sea bottom. The transducers of the profiler were facing upward so that the vertical distributions of the velocity profile in the entire water column were recorded, as well as water level elevations. The records were taken every hour with 1800 samples, with a resolution of 0.001 m s^{-1} and an accuracy of ±1% of measured values ±0.5 cm s^{-1}. The measurements were carried out 2.7 km off the coast, at the position 54°50.48′N, 17°53.09′E, where the water depth amounts to $h = 17$ m. The velocities were measured in 1 m thick layers. Velocity measurements in the superficial layers of the water column are less reliable due to disturbances caused by waves.

Wind velocities and directions were recorded using a cup anemometer installed on a mast near CRS Lubiatowo, on land, about 150 m from the shoreline, at the position 54°48.70′N, 17°50.43′E. The wind velocity measured over the land W_{land} was recalculated to obtain the wind velocity over the sea by the following formulas (Stella, 2021):

$$W_{\text{sea}} = 3.68\, W_{\text{land}} \quad \text{for} \quad W_{\text{land}} \le 1\ \text{m s}^{-1} \tag{1}$$

$$W_{\text{sea}} = 1.76\, W_{\text{land}} + 1.92\ [\text{m s}^{-1}] \quad \text{for} \quad W_{\text{land}} > 1\ \text{m s}^{-1} \tag{2}$$

The period of the measurements is too short to record the wind–wave–current parameters occurring in different seasons and under variable wave dynamics. Therefore, it is impossible to present any features of the local wind–wave–current climate. The selected wind–wave–current situations are used to test the mathematical/theoretical model.

2.2 Theoretical model

2.2.1 Wind-driven current

The logarithmic distribution of the steady flow velocity results from the Boussinesq hypothesis, where the shear stress $\tau(z)$ is assumed as $\tau = \rho u_f^2$, and the turbulent viscosity parameter $\nu_t(z)$ is assumed to increase linearly from zero at the sea bottom (see e.g. Ostrowski et al., 2018). This leads to the following well-known logarithmic velocity profile:

$$u(z) = \frac{u_f}{\kappa} \ln\left(\frac{z}{z_0}\right) \quad \text{for}\, z \ge z_0 \tag{3}$$

in which z_0 denotes the ordinate where $u = 0$, while κ is assumed equal to about 0.4 (see e.g. Kondo and Sato, 1982), and z_0 is the roughness height, typically $z_0 = k_N/30$ (k_N stands for the Nikuradse equivalent roughness).

The surface current velocity triggered by the wind, u_{surface}, can be determined from the velocity of the wind W_{sea} in the following way (Stella et al., 2019):

$$\begin{aligned} u_{\text{surface}} &= 0.03\, W_{\text{sea}} \quad && \text{for } W_{\text{sea}} < 8\ \text{m s}^{-1} \\ u_{\text{surface}} &= 0.035\, W_{\text{sea}} \quad && \text{for } W_{\text{sea}} \ge 8\ \text{m s}^{-1} \end{aligned} \tag{4}$$

Knowing the superficial flow velocity u_{surface} and using the logarithmic distribution described by Eq. (3) with

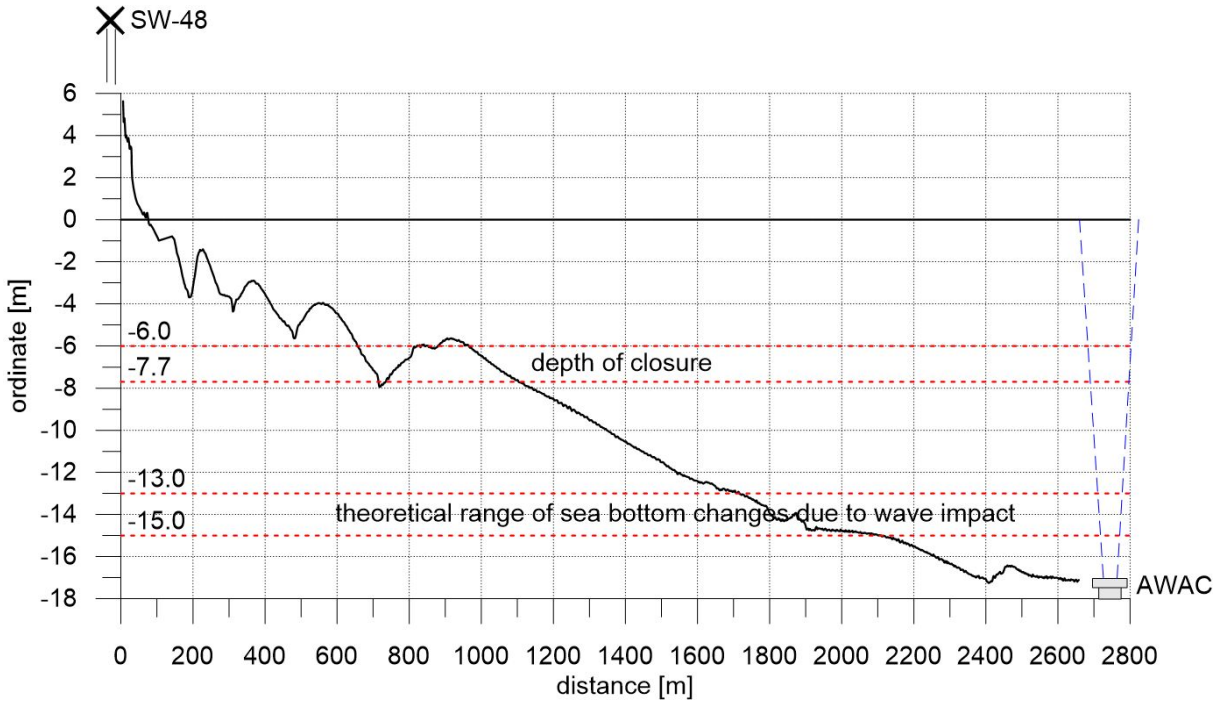

Figure 2. Exemplary cross-section of the shore at CRS Lubiatowo, the depth of closure (Cerkowniak et al., 2015a), the theoretical range of bottom level changes due to wave impact (Cerkowniak et al., 2015b) and the location of the measuring equipment.

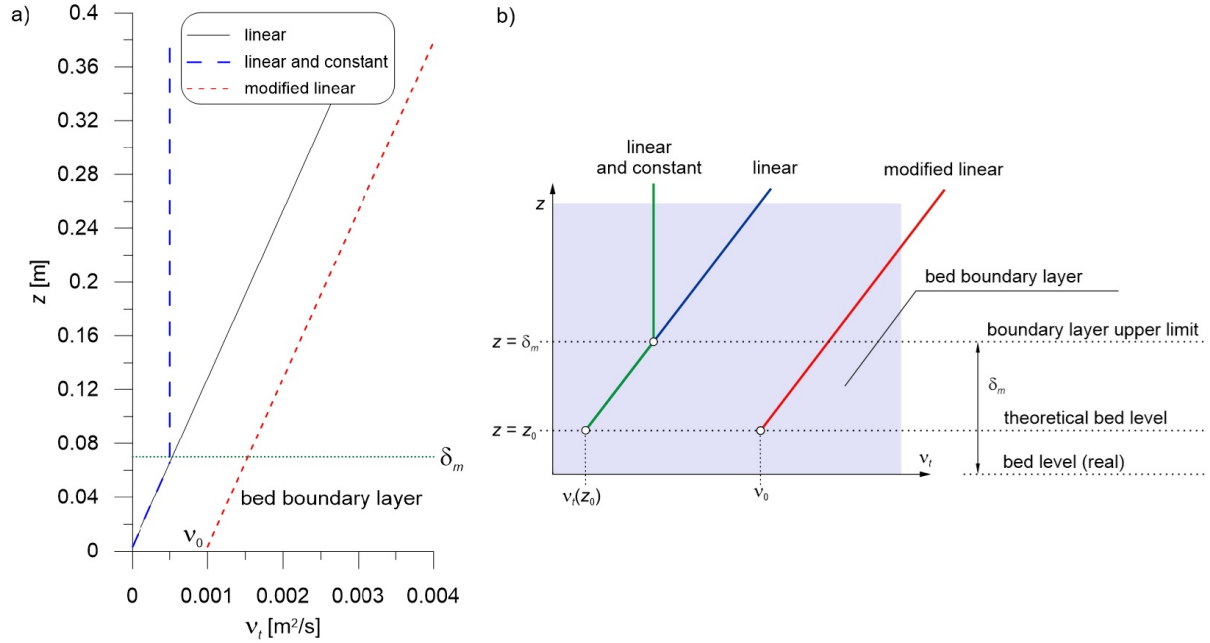

Figure 3. Turbulent kinematic viscosity $\nu_t(z)$ distributions, values determined by Ostrowski and Stella-Bogusz (2023), $z_0 = 0.0033$ m, $\delta_m = 0.07$ m and $\nu_0 = 0.001$ m (a); nearbed distributions of turbulent kinematic viscosity $\nu_t(z)$ (b).

$z = h$ and $u(h) = u_{\text{surface}}$, one can calculate the friction velocity u_f. After rearrangement, the following formula is obtained:

$$u_f = \frac{\kappa u_{\text{surface}}}{\ln\left(\frac{h}{z_0}\right)} \quad \text{for } z \geq z_0 \tag{5}$$

The stationary flow model should be supplemented with the hydrodynamic effect of the WBL. This impact was taken into account by Nielsen (1992), who implemented an apparent bottom roughness higher than the natural roughness of a rippled seabed. Stella et al. (2019) showed that the logarithmic distribution accurately reproduces the steady flow if the wind-driven current predominates. As already mentioned, the logarithmic velocity profile is obtained assuming that the turbulent kinematic viscosity v_t grows linearly upwards from the bottom level (see Figure 3a). For wave-dominated flows, following Brevik (1981), Stella et al. (2019) proposed a two-layer distribution of v_t. In the present study, in order to reproduce additional wave-induced nearbed shear stresses, a non-zero value of v_t, resulting from the impact of the WBL (as in Ostrowski and Stella-Bogusz, 2023) and the WCBL (proposed herein), is assumed at the theoretical bed level, i.e. for $z = z_0$ (see Figure 3).

The modified linear distribution of the turbulent kinematic viscosity v_t is described by the equation:

$$v_t = \kappa u_f (z - z_0) + v_0 \quad \text{for } z \geq z_0 \tag{6}$$

Consequently, the flow velocity $u(z)$ description by the modified logarithmic vertical distribution reads as:

$$u(z) = \frac{u_f}{\kappa} \ln\left(\frac{\kappa u_f (z - z_0) + v_0}{v_0}\right) \quad \text{for } z \geq z_0 \tag{7}$$

where a non-zero turbulent kinematic viscosity v_0 at the theoretical bed level is resolved by the equation of motion in the wave or the wave–current bed boundary layer.

For a known superficial velocity u_{surface}, the friction velocity u_f (and shear stress $\tau = \rho u_f^2$) can be estimated using the modified logarithmic profile described by Eq. (7) with $u(h) = u_{\text{surface}}$. Unlike Eq. (3), Eq. (7) ought to be solved numerically.

In the classical logarithmic description, $v_t(z_0) = \kappa u_f z_0$. If $v_t(z_0)$ exceeds the value of v_0, the modified logarithmic approach should not be applied, since the impact of the WBL is negligibly small.

2.2.2 Wave turbulent bed boundary layer

In the present study, the integral momentum method of Fredsøe (1984) is used to solve the momentum equation in the WBL or (alternatively) the WCBL. According to this approach, the momentum equation is integrated over the boundary layer thickness δ, from the ordinate $z_0 = k_N/30$ to the ordinate $\delta + z_0$. Assumption of the logarithmic velocity profile in the wave boundary layer (characterised by the wave-related friction velocity u_{f_w}) and introduction of the dimensionless variable

$$z_1 = \frac{U}{u_{f_w}} \kappa \tag{8}$$

leads to the equation (Fredsøe, 1984):

$$\frac{d(z_1)}{d(\omega t)} = \frac{30\kappa^2 U}{k_N \omega \left[e^{z_1}(z_1 - 1) + 1\right]} - \frac{z_1 (1 + z_1 - e^{z_1})}{e^{z_1}(z_1 - 1) + 1} \frac{1}{U} \frac{dU}{d(\omega t)} \tag{9}$$

in which $U(\omega t)$ is the wave-induced velocity (the so-called free-stream velocity) at the WBL upper limit, and $\omega = 2\pi/T$ is the angular frequency of wave motion with the period T.

The velocity $U(\omega t)$ depends on the wave height H, wave period T and wavelength L. The length is found from the dispersion relationship, which takes into account the interaction of waves with the superficial flow and has the following form (Nielsen, 2009):

$$\left(\frac{2\pi}{T} - \frac{2\pi}{L} u_{\text{surface}} \cos\gamma\right)^2 = g \frac{2\pi}{L} \tanh\left(\frac{2\pi}{L} h\right) \tag{10}$$

where γ denotes an angle between the directions of the steady current and wave propagation, while g is the standard acceleration of gravity.

Eq. (9) must be solved numerically. Solution of Eqs. (8) and (9) yields the friction velocity $u_{fw}(\omega t)$ in the turbulent WBL and its thickness $\delta(\omega t)$:

$$\delta = \frac{k_N}{30}(e^{z_1} - 1) \tag{11}$$

The quantity $\delta_m = \delta(\omega t = \pi/2)$ at the moment corresponding to the wave crest (or trough) is assumed as the characteristic WBL thickness, representative of the entire wave period T. It has also been assumed that the root-mean-square wave friction velocity $u_{fw,\text{RMS}}$ is the value of u_{fw} representative of the wave period T.

The turbulent kinematic viscosity in the turbulent WBL is described by the following linear distribution:

$$v_{tw} = \kappa u_{fw,\text{RMS}} z \tag{12}$$

The wave-generated turbulent kinematic viscosity at the top of the WBL constitutes the bottom value of this

parameter (v_0) in the wind-driven flow model. Hence, for $v_{tw}(z=\delta_m)=v_0$. Consequently, one has:

$$v_0 = \kappa u_{fw,\mathrm{RMS}} \delta_m \tag{13}$$

The value of v_0 calculated with the above formula is then used in Eq. (7).

2.2.3 Wave-current turbulent bed boundary layer

In the wave-current flow, the friction velocity u_f related to the shear stress induced by the steady current appears at the top of the bed boundary layer. For such a case, Fredsøe (1984) derived the following differential equation:

$$\frac{d(z_1)}{d(\omega t)} = \frac{z_1(1+z_1-e^{z_1})}{e^{z_1}(z-1)+1}\frac{1}{U}\frac{dU}{d(\omega t)} + \\ + \frac{30\kappa}{k_N}\frac{\sqrt{\kappa^2U^2+z_1^2u_f^2+2z_1\kappa u_f U\cos\gamma}}{\omega\left[e^{z_1}(z_1-1)+1\right]} \tag{14}$$

After solving Eq. (14), i.e. after calculating the variable $z_1(\omega t)$, one can determine the friction velocity in the WCBL $u_{fwc}(\omega t)$ by using the auxiliary variable $u_f^*(\omega t)$ from the following equations (Fredsøe, 1984):

$$z_1 = \frac{U\kappa}{u_f^*} \tag{15}$$

$$\frac{1}{u_f^*} = \frac{u_f\cos\gamma}{u_{fwc}^2-u_f^2} + \sqrt{\frac{u_f^2\cos^2\gamma}{\left(u_{fwc}^2-u_f^2\right)^2}+\frac{1}{u_{fwc}^2-u_f^2}} \tag{16}$$

Rearrangement of Eq. (16) yields the following formula, describing the friction velocity in the wave-current turbulent bed boundary layer:

$$u_{fwc} = \sqrt{u_f^2+\left(u_f^*\right)^2+2u_f^*u_f\cos\gamma} \tag{17}$$

The angle $\phi(\omega t)$ between the wind-driven current and the resultant wave-current shear stress in the bed boundary layer is given as follows (Fredsøe, 1984):

$$\phi = \arcsin\left(\frac{u_f^*}{u_{fwc}}\sin\gamma\right) \tag{18}$$

Equation (14), similarly to Eq. (9), requires a numerical solution with the initial condition $z_1=0$ for $\omega t=0$. Eqs. (9) and (14) are singular for $\omega t=0$. An approximate solution of Eq. (14) for small values of ωt has the following form (Fredsøe, 1984):

$$z_1 = \sqrt{\frac{2}{3}\beta\omega t} \tag{19}$$

in which

$$\beta = \frac{60\kappa u_f}{\omega k_N} \tag{20}$$

In the first step of computations, namely for $\omega t = 0+\Delta\omega t$, the quantity z_1 should be determined using Eqs. (19) and (20).

As in the case of the WBL, the thickness of the WCBL can be calculated with Eq. (11). Unlike in pure sinusoidal wave motion, the variability of parameters of the wave-current boundary layer (friction velocity and layer thickness) during the wave crest is different from those during the wave trough. The boundary layer thickness representative of the wave period is proposed as $\delta_m=\max(\delta_1,\delta_2)$, where δ_1 and δ_2 represent the thicknesses of the boundary layer at moments corresponding to extreme velocities at the top of the boundary layer in the phases of wave crest and trough, respectively. For the sinusoidal wave, this denotes $\delta_1=\delta(\omega t=\pi/2)$ and $\delta_2=\delta(\omega t=3\pi/2)$. The turbulent kinematic viscosity at the theoretical bed level $v_t(z_0)$ is described by Eq. (13), as for the wave boundary layer.

The quantity u_f in Eq. (14) is determined from Eq. (7). The quantity v_0 in Eq. (7) is yielded by Eq. (14). Therefore, in order to find the wind-driven current velocity distribution incorporating the impact of the bed wave-current boundary layer, an iterative approach is necessary. The proposed iterative procedure is described as follows:

1. Determination of u_f with Eq. (5)
2. Calculation of $u_{fwc}(\omega t)$ by solution of Eqs. (14), (15) and (17)
3. Calculation of $u_{fwc,\mathrm{RMS}}$
4. Calculation of $\delta(\omega t)$ with Eq. (11) and then $\delta_1=\delta(\omega t=\pi/2)$ and $\delta_2=\delta(\omega t=3\pi/2)$
5. Determination of $\delta_m=\max(\delta_1,\delta_2)$
6. Calculation of v_0 with Eq. (13), substituting $u_{fw,\mathrm{RMS}}=u_{fwc,\mathrm{RMS}}$
7. Determination of u_f by solution of Eq. (7)
8. Return to point 2.

The iterative procedure is continued until the friction velocity u_f coincides with its final value (with an assumed accuracy, e.g. 0.0001 m s^{-1}).

Figure 4 shows exemplary results of computations carried out for typical storm wave conditions in the Baltic

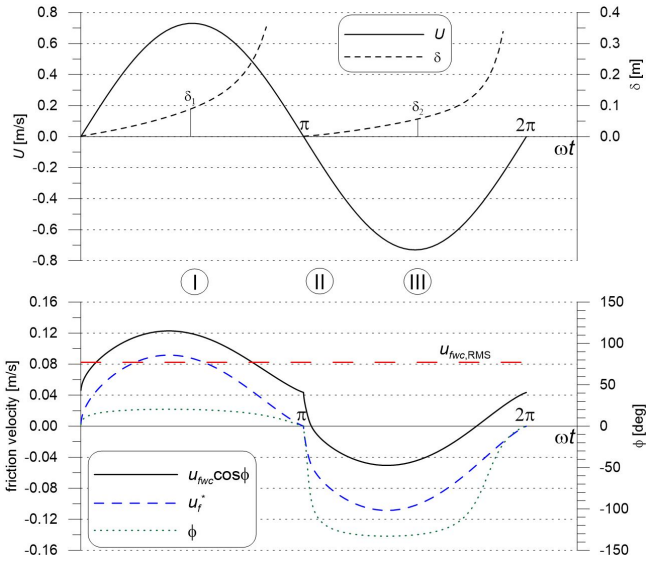

Figure 4. Free stream velocity U, wave-current bed boundary layer thickness δ, angle ϕ, friction velocities u_{fwc} and u_f^* determined by the integral momentum method of Fredsøe (1984) for $H = 3$ m, $T = 8$ s, $u_{\text{surface}} = 0.5$ m s^{-1}, $\gamma = 30°$, $h = 17$ m and $k_N = 0.1$ m.

Sea, with the wave height and period equal to $H = 3$ m and $T = 8$ s, respectively, wind-driven current with the superficial velocity $u_{\text{surface}} = 0.5$ m s^{-1} at an angle of $\gamma = 30°$ with respect to the direction of wave propagation, for the water depth $h = 17$ m and the bed roughness $k_N = 0.1$ m (corresponding to the ripple height observed at that site). Symbols I, II and III denote the phases of the wave crest, wave-induced flow reversal and wave trough, respectively.

A scheme presenting the wave free stream velocity U, the wind-driven flow velocity $u(z = \delta_m)$, the instantaneous resultant velocity $u_{\text{resultant}}$ and the instantaneous resultant friction velocity u_{fwc} in the turbulent wave-current bed boundary layer is given in Figure 5.

Figure 6 shows the classical logarithmic distribution of the wind-driven flow velocity described by Eq. (3) and modified logarithmic profiles given by Eq. (7). The modified profiles are shown for two variants: (a) taking into account the impact of the wave bed boundary layer and (b) taking into account the impact of the wave-current bed boundary layer. The computations have been carried out for the previously assumed typical Baltic storm conditions ($H = 3$ m, $T = 8$ s, $u_{\text{surface}} = 0.5$ m s^{-1}, $\gamma = 30°$, $h = 17$ m and $k_N = 0.1$ m).

The computational results presented in Figure 6 imply that an increase in the nearbed turbulent kinematic viscosity due to the impact of the wave boundary layer (WBL) or the wave-current boundary layer (WCBL), which significantly increases the friction velocity u_f, results in a distinct reduction of the velocities in the entire water column. It should be noted that the difference between the

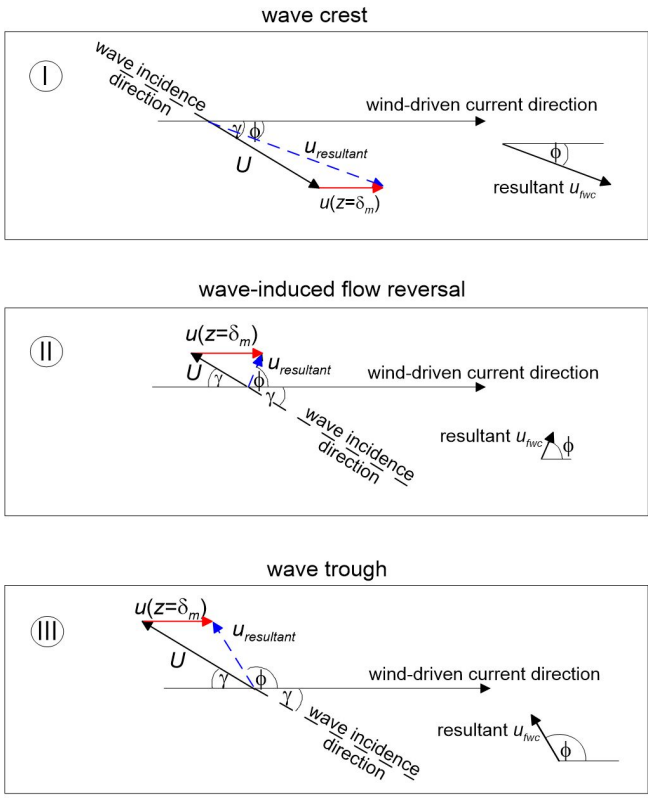

Figure 5. Wave free stream velocity U, wind-driven flow velocity $u(z = \delta_m)$, resultant velocity and the instantaneous resultant friction velocity uf in turbulent wave-current bed boundary layer.

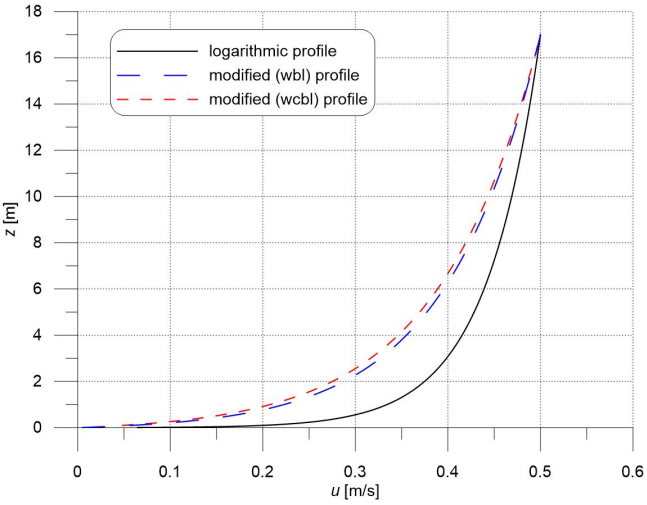

Figure 6. Logarithmic velocity profile and two modified logarithmic profiles: with impacts of the wave boundary layer (WBL) and the wave-current boundary layer (WCBL) for $H = 3$ m, $T = 8$ s, $u_{\text{surface}} = 0.5$ m s^{-1}, $\gamma = 30°$, $h = 17$ m and $k_N = 0.1$ m.

curves depicting the WBL impact and the WCBL impact is relatively small.

3. Results and discussion

Computations were carried out for more than 1000 sets of wind-wave parameters measured at the study site from 26 April to 30 June 2014. The data represent both wave-dominated and current-dominated hydrodynamic conditions. Figures 7–9 show examples of recorded time-averaged (over 2 minutes) velocity profiles and theoretical distributions, i.e. traditional logarithmic profiles and modified logarithmic profiles in two variants (WBL and WCBL). In the figure captions, the symbols H_s and T_p denote the significant wave height and the wave energy peak period, respectively. The measured velocities (dots) represent values for 1 m thick layers. These values come directly from the measuring device.

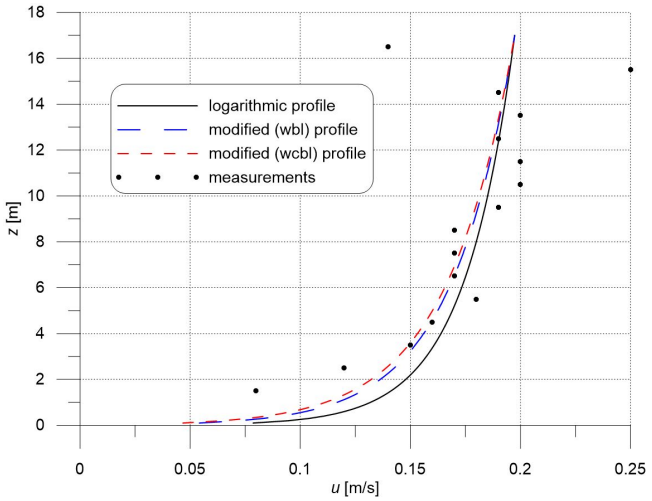

Figure 7. Theoretical and measured mean velocity profiles ($H_s = 1$ m, $T_p = 4.9$ s, $u_{\text{surface}} = 0.197$ m s^{-1}, $\gamma = 47.3°$, $h = 17$ m, $k_N = 0.1$ m).

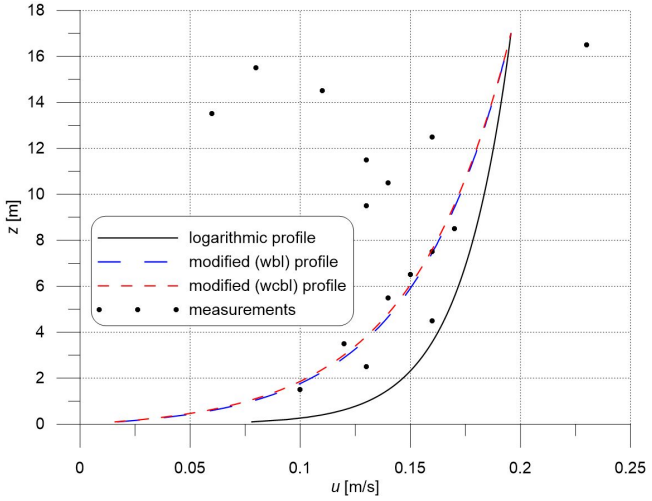

Figure 8. Theoretical and measured mean velocity profiles ($H_s = 2.4$ m, $T_p = 7.9$ s, $u_{\text{surface}} = 0.196$ m s^{-1}, $\gamma = 45.95°$, $h = 17$ m, $k_N = 0.1$ m).

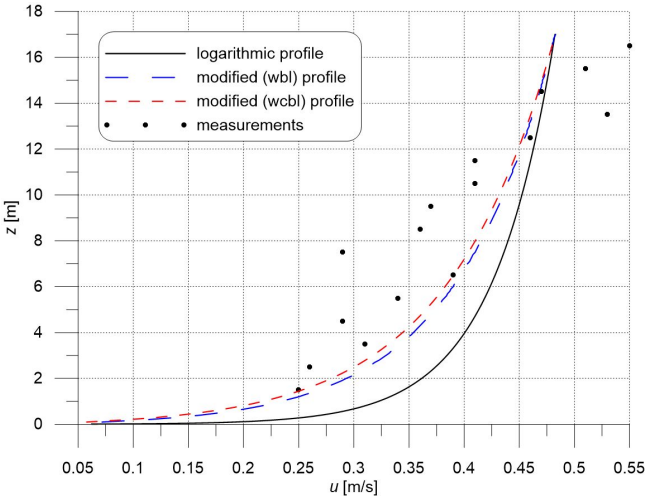

Figure 9. Theoretical and measured mean velocity profiles ($H_s = 2.1$ m, $T_p = 7.7$ s, $u_{\text{surface}} = 0.483$ m s^{-1}, $\gamma = 19.14°$, $h = 17$ m, $k_N = 0.1$ m).

In the cases presented in Figures 7 and 8 the recorded wind speeds and directions with respect to the wave propagation directions were very similar. The calculated superficial velocities of the wind-driven current are therefore almost identical. The wave conditions, however, were considerably different. The hydrodynamic regime was current-dominated in the first case but wave-dominated in the second.

In the first case, the modified logarithmic distributions do not differ much from the classical logarithmic distribution (Figure 7), as the wave-induced impact is insignificant due to the small value of the near-bed turbulent kinematic viscosity ν_0. Hence, the distribution of the turbulent kinematic viscosity is similar to that yielding the classical logarithmic distribution.

Under wave-dominated conditions, the modified logarithmic distributions differ significantly from the traditional logarithmic model. The modified logarithmic profiles yield distinctly lower velocities, particularly in areas closer to the bottom (Figure 8). As already mentioned, this results from additional bed friction caused by the turbulent bed boundary layer of either wave or wave-current type. The modified logarithmic distributions appear to reproduce the measurements better than the conventional logarithmic approach does.

Figure 9 shows velocity profiles from the theoretical models and measurements for the case of a strong current (with a superficial velocity of almost 0.5 m s^{-1}) interacting with relatively high collinearly propagating waves. The modified velocity distributions yield distinctly smaller values, closer to the field data than those of the logarithmic distribution.

The computational results show that the impact of the wave boundary layer (WBL) on the mean velocity distribution does not differ much from that of the wave–current

boundary layer (WCBL). This is because, as pointed out by Nielsen (1992, 2009), the steady current weakly affects the wave bed boundary layer. Therefore, in wave-dominated flow regimes, the WBL and WCBL velocity profiles are almost identical (see Figure 8).

The differences between the theoretical and measured profiles may result from the randomness of wave-current marine processes. For instance, wave parameters are applied in the model as representative values for actually irregular waves, namely H_s and T_p. Some discrepancies between the theory and field data are certainly caused inaccuracies in the measuring device. Secondly, the modelling system itself (as many other theoretical models) contains simplifications, e.g. with respect to near-bed turbulent processes and generation of wind-driven current (the latter model does not account for sea surface roughness). Such imperfections can contribute to discrepancies between the modelled and measured velocities.

Further, the velocity values at ordinates closer to the sea bottom would be useful for the analysis. Unfortunately, such measurements could not be carried out due to technical limitations (the height of the frame on which the instrument was mounted and the so-called blanking distance i.e. the water layer directly in front of the transducers where measurement accuracy is not acceptable). The velocity data in the surface water layer (up to 10% of the total depth) are not fully reliable due to side-lobe interference. Measurements taken in this layer are therefore excluded from consideration.

4. Conclusions

The paper presents a theoretical model of the wave-driven flow interacting with waves in the remote foreshore, defined as a coastal region located beyond the depth of closure. The newly developed modified logarithmic velocity distribution has been tested against field data. It appears that the shape of the velocity profile is distinctly affected by the presence of near-bed wave-induced oscillations constituting the turbulent bed boundary layer. On the basis of the conducted analysis, the following major conclusions can be drawn:

- The wave bed boundary layer or the wave-current bed boundary layer produces additional turbulent bed shear stresses, represented in the wind-driven flow model by a modified linear distribution of the turbulent kinematic viscosity.
- The above modification, together with the solution of the motion equation in the bed boundary layer, yields a modified logarithmic profile of the wind-driven flow velocity.
- The reduction of flow velocities near the bottom, particularly distinct under the wave-dominated regime, is the main feature of the new model. This theoretical finding is consistent with the field data.
- The computational results show that including the wave bed boundary in the wind-driven flow model yields almost the same effect as including the wave-current boundary layer. Hence, it is confirmed that the wave-induced near-bed turbulence strongly affects the wind-driven current, whereas the influence of the wind-driven current on the bed boundary layer is insignificant.

The authors hope that the present study advances investigations of hydrodynamic processes occurring in the remote foreshore zone of non-tidal seas. This coastal region is located beyond the depth of closure – at depths of 15–20 m in the case of the Baltic Sea. The proposed theoretical modelling scheme can help determine the forces driving sediment transport and thereby improve predictions of seabed dynamics, including the development and migration of sandy bed forms. The obtained results may stimulate further research on the remote foreshore morphodynamics presented by Stella (2021). Knowledge of hydro-, litho-, and morphodynamic parameters in the remote foreshore is useful in planning marine engineering projects, e.g. wind farms. However, in view of the climate change perspective – in the context of planning marine investments – it will probably be necessary to consider potential changes in local wave-current characteristics that could require modifications of the proposed theoretical approach.

The presented theoretical approach can be applied to any other non-tidal basins at locations beyond surf zones (where wave breaking and wave-driven currents predominate) and beyond large water depths (where typical offshore phenomena occur, such as the Ekman spiral). The theoretical model of the wind-driven current includes additional wave-induced bed shear stresses overlapping with those associated with the classical impact of bottom roughness and friction.

Further investigations of these topics will continue, involving, among other activities, wave-current measurements and sea bed observations. Such activities are currently conducted near CRS Lubiatowo using a DWR4 ACM buoy (a Directional Waverider buoy with an Acoustic Current Meter, deployed at a depth of 18 m, 2.8 km from the shoreline), a side-scan sonar, and a multi-beam echosounder (Sidescan Sonar Klein 3900 and Multibeam Reson SeaBat 8101, respectively), in the experimental area, rectangular in shape and located parallel to the shoreline, with dimensions of 2.6 × 0.53 km, at depths of 16–20 m.

Acknowledgements

The research was partially funded by the Ministry of Science and Higher Education, Poland, under IBW PAN

mission-related programme No. 2 ("Dynamics of Coastal-Estuarine Zone") and partially by the National Science Centre, Poland, within the research project No. 2021/41/B/ST8/01943 ("Dynamics of the bottom in the remote foreshore of a non-tidal sea"), which are hereby gratefully acknowledged.

Conflict of interest

None declared.

References

Baas, J., Malarkey, J., Lichtman, I., Amoudry, L., Thorne, P., Hope, J., Peakall, J., Paterson, D., Bass, S., Cooke, R., Manning, A., Parsons, D., Ye, L., 2021. *Current- and Wave-Generated Bedforms on Mixed Sand–Clay Intertidal Flats: A New Bedform Phase Diagram and Implications for Bed Roughness and Preservation Potential*. Front. Earth Sci. 9. https://doi.org/10.3389/feart.2021.747567

Brevik, I., 1981. *Oscillatory rough turbulent boundary layers*. J. Waterw. Port Coast. Ocean Div. 107 (3), 175–188. https://doi.org/10.1061/JWPCDX.0000261

Cerkowniak, G.R., Ostrowski, R., Stella, M., 2015a. *Depth of closure in the multi-bar non-tidal nearshore zone of the Baltic Sea: Lubiatowo (Poland) case study*. Bull. Maritime Inst. Gdańsk, 30 (1), 180–188. http://doi.org/10.5604/12307424.1185577

Cerkowniak, G.R., Ostrowski, R., Stella, M., 2015b. *Wave-Induced Sediment Motion Beyond the Surf Zone: Case Study of Lubiatowo (Poland)*. Arch. Hydro-Eng. Environ. Mech. 62 (1–2), 27–39.

Cerkowniak, G.R., Ostrowski, R., Pruszak, Z., 2017. *Application of Dean's curve to the investigation of the long-term evolution of the southern Baltic multi-bar shore profile*. Oceanologia 59 (1), 18–27. http://dx.doi.org/10.1016/j.oceano.2016.06.001

Chen, X., Hu, X., 2020. *Explicit approximation for velocity and sediment flux above mobile sediment bed beneath current and asymmetric wave*. Coastal Eng. 157. https://doi.org/10.1016/j.coastaleng.2020.103635

Dean, R.G., 2002. *Beach Nourishment. Theory and Practice*. Advanced Series on Ocean Engineering Vol. 18. World Sci. Publ. Co. Pte. Ltd., 399 pp. https://doi.org/10.1142/2160

Egan, G., Cowherd, M., Fringer, O., Monismith, S., 2019. *Observations of near-bed shear stress in a shallow, wave- and current-driven flow*. J. Geophys. Res. 124, 6323–6344. https://doi.org/10.1029/2019JC015165

Fredsøe, J., 1984. *Turbulent boundary layer in combined wave-current motion*. J. Hydraulic Eng. 110 (HY8), 1103–1120. https://doi.org/10.1061/(ASCE)0733-9429(1984)110:8(1103)

Grant, W.D., Madsen, O.S., 1979. *Combined wave and current interaction with a rough bottom*. J. Geophys. Res. 84 (C4), 1797–1808. https://doi.org/10.1029/JC084iC04p01797

Kemp, P., Simons, R., 1982. *The interaction between waves and a turbulent current: Waves propagating with the current*. J. Fluid Mech. 116, 227–250. https://doi.org/10.1017/S0022112082000445

Kondo, J., Sato, T., 1982. *The Determination of the von Kármán Constant*. J. Meteorol. Soc. Japan, 60 (1), 461–471.

Krauss, W., 2001. *Chapter: Baltic sea circulation*. [In:] *Encyclopedia of Ocean Sciences*. https://doi.org/10.1006/rwos.2001.0381

Lacy, J.R., Rubin, D.M., Ikeda, H., Mokudai, K., Hanes, D.M., 2007. *Bed forms created by simulated waves and currents in a large flume*. J. Geophys. Res. 112, C10018. https://doi.org/10.1029/2006JC003942

Lim, K.Y., Madsen, O.S., 2016. *An experimental study on near-orthogonal wave–current interaction over smooth and uniform fixed roughness beds*. Coast. Eng. 116, 258–274. https://doi.org/10.1016/j.coastaleng.2016.05.005

Malarkey, J., Davies, A.G., 1998. *Modelling wave–current interactions in rough turbulent bottom boundary layers*. Ocean Eng. 25, 119–141. https://doi.org/10.1016/S0029-8018(96)00062-5

Meyer, Z., 2009. *Modified Logarithmic Tachoida Applied to Sediment Transport in a River*. Acta Geophysica 57 (3), 743–759. https://doi:10.2478/s11600-009-0010-0

Nielsen, P., 1992. *Coastal bottom boundary layers and sediment transport*. Advanc. Ser. Ocean Eng., Vol 4, World Sci. Publ. Co. Pte. Ltd., 340 pp. https://doi.org/10.1142/1269

Nielsen, P., 2009. *Coastal and Estuarine Processes*. Advanc. Ser. Ocean Eng., Vol 29, World Sci. Publ. Co. Pte. Ltd., 343 pp. https://doi.org/10.1142/7114

Ostrowski, R., Schönhofer, J., Szmytkiewicz, P., 2016. *South Baltic representative coastal field surveys, including monitoring at the Coastal Research Station in Lubiatowo, Poland*. J. Marine Syst. 162, 89–97. https://doi.org/10.1016/j.jmarsys.2015.10.006

Ostrowski, R., Stella, M., 2020. *Potential dynamics of non-tidal sea bed in remote foreshore under waves and currents*. Elsevier Science B.V., 207 pp. https://doi.org/10.1016/j.oceaneng.2020.107398

Ostrowski, R., Stella-Bogusz, M., 2023. *Modified logarithmic distribution of wind-driven flow velocity in remote foreshore of the non-tidal sea*. Oceanologia, 65 (4), 556–563. https://doi.org/10.1016/j.oceano.2023.06.003

Ostrowski, R., Stella, M., Szmytkiewicz, P., Kapiński, J., Marcinkowski, T., 2018. *Coastal hydrodynamics beyond the surf zone of the south Baltic Sea*. Oceanologia, 60 (3),

264–276.
https://doi.org/10.1016/j.oceano.2017.11.007

Overes, P.H.P., Borsje, B.W., Luijendijk, A.P., Hulscher, S.J.M.H., 2024. *The importance of time-varying, non-tidal currents in modelling in-situ sand wave dynamics*. Coast. Eng. 189, 104480.
https://doi.org/10.1016/j.coastaleng.2024.104480

Pruszak, Z., Szmytkiewicz, P., Ostrowski, R., Skaja, M., Szmytkiewicz, M., 2008. *Shallow-water wave energy dissipation in a multi-bar coastal zone*. Oceanologia, 50 (1), 43–58.

Reyes-Hernández, C., Valle-Levinson, A.. 2010. *Wind Modifications to Density-Driven Flows in Semienclosed, Rotating Basins*. J. Phys. Oceanogr. 40, 1473–1487.
https://doi.org/10.1175/2010JPO4230.1

Stella, M., 2021. *Morphodynamics of the south Baltic seabed in the remote nearshore zone in the light of field measurements*. Mar. Geol.
https://doi.org/10.1016/j.margeo.2021.106546

Stella, M., Ostrowski, R., Szmytkiewicz, P., Kapiński, J., Marcinkowski, T., 2019. *Driving forces of sandy sediment transport beyond the surf zone*. Oceanologia, 61 (1), 50–59.
https://doi.org/10.1016/j.oceano.2018.06.003

Trzeciak, S., 2000. *Marine Meteorology with Oceanography*. Wyd. Nauk. PWN, 249 pp., (in Polish).

van Rijn, L.C., 1993. *Principles of Sediment Transport in Rivers, Estuaries and Coastal Seas*. Vol. 1006. Aqua Publ., Amsterdam.

Wiberg, P.L., 2005. *Wave-Current Interaction*. [In:] *Encyclopedia of Coastal Science*, Schwartz, M.L. (Ed.), Encyclopedia Earth Sci. Ser., Springer, Dordrecht.
https://doi.org/10.1007/1-4020-3880-1_343

Zuo, L.Q., Roelvink, D., Lu, Y.J., 2019. *The mean suspended sediment concentration profile of silty sediments under wave-dominant conditions*. Cont. Shelf Res. 186, 111–126.
https://doi.org/10.1016/j.csr.2019.07.016